Transmembrane 163 (TMEM163) protein effluxes zinc

Vanessa B. Sanchez[1], Saima Ali[1], and Math P. Cuajungco[1,2,*]

[1]Department of Biological Science, and [2]Center for Applied Biotechnology Studies, California State University Fullerton, CA, USA 92831

Running Title: *TMEM163 effluxes zinc*

***To whom correspondence should be addressed**: Dr. Math P. Cuajungco: Department of Biological Science, California State University Fullerton, 800 North State College Blvd, Fullerton, CA 92831. E-mail: mcuajungco@fullerton.edu; Tel: +1-657-278-8522; Fax: +1-657-278-3426.

Keywords: SV31, cation diffusion facilitator, synaptic vesicle, lysosome, single nucleotide polymorphism, zinc transporter

Background: Previous studies using rodent Tmem163 showed that it binds and transports zinc. However, it is not known whether the protein serves as an influx or efflux transporter. Using human TMEM163, we set out to show its function in cells.
Results: Zinc flux assays using Newport Green and Fluozin-3 fluorescence dyes revealed that cells stably or transiently expressing TMEM163 exhibited marked decrease of cytoplasmic zinc levels. Site-directed mutagenesis of key amino acid residues known as zinc-binding sites or are predicted as post-translational modification sites disrupted zinc efflux.
Conclusion: TMEM163 is a zinc efflux transporter, but is predicted to be structurally distinct to known ZnT efflux transporters.
Significance: TMEM163 may represent a new subclass member of the cation diffusion facilitator family of zinc transporter that is vital for zinc homeostasis in specific cell types.

ABSTRACT

Recent investigations of rodent Tmem163 protein suggest that it binds to and transports zinc as a dimer, and that alanine mutagenesis of its two conserved aspartate (D123A/D127A) residues perturbs its function. Direct evidence, however, is lacking whether it is an influx or efflux transporter. We hypothesized that human TMEM163, like its rodent counterpart, is a zinc effluxer. Using cultured human cell lines that either stably or transiently expressed TMEM163 protein, we determined the direction of zinc flux using two distinct fluorescent dyes. Spectrofluorometric assays showed that TMEM163-expressing cell lines loaded with zinc markedly reduced intracellular zinc levels when compared with controls. The specificity of the fluorescence signal was confirmed upon treatment with TPEN, a high-affinity zinc chelator. To further dissect the function of TMEM163, we performed alanine mutagenesis of two similarly conserved aspartate residues (D124A/D128A) to inactivate zinc efflux. We also performed site-directed mutagenesis of other conserved residues in TMEM163 (i.e. S61R, S95C, S193P, and E286K) to test their effects on the function of TMEM163. We found a significant reduction of zinc efflux activity upon expression of D124A/D128A or E286K mutation. Taken together, our findings demonstrate that TMEM163 is a zinc effluxer that contributes to zinc homeostasis in cells.

INTRODUCTION

Abnormal extracellular zinc accumulation leading to cytosolic zinc overload has been shown to result in cytotoxicity *in vitro* and *in vivo*, which can be rescued by zinc-specific chelators (Choi *et al.*, 1988; Koh and Choi, 1994; Cuajungco and Lees, 1996; Koh *et al.*,

1996; Cuajungco and Lees, 1998; Kukic *et al.*, 2014). Many tissues and organs, therefore, have redundant defense mechanisms to strictly maintain zinc homeostasis in order to prevent the cytotoxic effect of intracellular zinc elevation. Zinc homeostasis in mammalian cells is achieved by a tissue-specific and highly conserved low molecular weight zinc transport protein families called ZNT (SLC30, solute carrier 30A) and Zrt- and Irt-like protein (ZIP; SLC39) (Eide, 2006; Colvin *et al.*, 2010; Kambe *et al.*, 2014). The ZNT proteins are known to efflux zinc from the cytoplasm into the extracellular milieu and into the lumen of membrane-bound or vesicular compartments. The ZIP proteins, meanwhile, influx zinc from the outside of the cell into the cytoplasm and from the lumen of membrane-bound or vesicular compartments into the cytoplasm (Eide, 2006; Colvin *et al.*, 2010; Kambe *et al.*, 2014). In addition to ZNTs, the cells have secondary defense mechanisms to prevent cytoplasmic zinc overload and buffer intracellular zinc elevation, which is accomplished by metallo-proteins, amino acids such as histidine and cysteine, as well as small proteins such as metallothionein (MT) and glutathione (Itoh *et al.*, 1983; Aiken *et al.*, 1992; Horn *et al.*, 1995).

Zinc dyshomeostasis has been implicated in several human diseases such as schizophrenia (Scarr *et al.*, 2016), age-related macular degeneration (Smailhodzic *et al.*, 2014), Alzheimer's disease (Cuajungco and Lees, 1997a; b; Danscher *et al.*, 1997; Cuajungco *et al.*, 2000; Beyer *et al.*, 2009; Bosomworth *et al.*, 2013), Parkinson's disease-like dystonia (Aydemir *et al.*, 2017), amyotrophic lateral sclerosis (Kim *et al.*, 2009; Kaneko *et al.*, 2015), multiple sclerosis (Choi *et al.*, 2016), cerebral stroke (Koh *et al.*, 1996; Yoo *et al.*, 2004; Medvedeva *et al.*, 2009), and Mucolipidosis type IV (MLIV) (Cuajungco and Lees, 1997b; Eichelsdoerfer *et al.*, 2010; Cuajungco *et al.*, 2014; Smailhodzic *et al.*, 2014; Scarr *et al.*, 2016). In the case of MLIV, a neurodegenerative disease caused by the loss-of-function mutation in the transient receptor potential mucolipin-1 (TRPML1) ion channel, we found abnormal lysosomal zinc accumulation among zinc-treated MLIV patient fibroblasts and human embryonic kidney (HEK)-293 cells upon RNA interference (RNAi)-induced knock down of TRPML1 (Eichelsdoerfer *et al.*, 2010; Cuajungco *et al.*, 2014). We also observed increased tissue zinc levels in post-mortem brain of Trpml1-null mice (Eichelsdoerfer *et al.*, 2010). Our interest in human TMEM163 stemmed from these observations and our recent finding that TMEM163 interacts with TRPML1 (Cuajungco *et al.*, 2014). Rodent Tmem163, also known as synaptic vesicle 31 (SV31), was first identified from rat brain synaptosomes using proteomics analysis and was shown to bind zinc, nickel, and copper (Burre *et al.*, 2007). Tmem163 has been detected in certain types of glutamatergic and γ-aminobutyric acid (GABA)-ergic neuronal populations (Burre *et al.*, 2007; Barth *et al.*, 2011). Barth *et al.* (2007) used immunocytochemistry and subcellular fractionation studies of neuron-like PC-12 cells stably expressing rodent Tmem163 to reveal that this protein is detected mostly in the plasma membrane (PM), lysosomes, early endosomes, and other vesicular compartments especially synaptic vesicles (Barth *et al.*, 2011). Our analysis shows that TMEM163 transcripts are detected in many tissues, notably in the brain, lung, pancreas, kidney, ovary, and testis (Cuajungco *et al.*, 2014). Confocal microscopy studies of heterologously expressed TMEM163 in HEK-293 cells revealed PM and lysosomes localization (Cuajungco *et al.*, 2014).

Previously, it was shown that purified rodent Tmem163 protein reconstituted in liposomes was shown to dimerize and transport zinc (Waberer *et al.*, 2017). It was also shown that Tmem163's ability to bind and transport zinc is inactivated when two conserved aspartate residues are mutated into alanine (i.e. Tmem163-D123A/D127A). These mutations, however, do not affect the protein's dimerization. This particular study did not address the question of whether the protein serves to transport zinc in or out of living cells. In the current report, we reveal for the first time that human TMEM163 is a zinc efflux transporter using two zinc-specific fluorescent dyes. Amino acid substitution of conserved residues that could disrupt TMEM163's structure negatively affects zinc efflux activity. Taken together, these observations indicate that TMEM163 should be designated as a new member of the cation diffusion facilitator (CDF) family of zinc efflux transporters that are crucial to maintaining zinc homeostasis in living organisms.

MATERIALS AND METHODS

Bioinformatics Analysis

We performed bioinformatics analysis (www.expasy.org) of TMEM163 using TMPred (Hofmann and Stoffel, 1993) and TMRPres2d (Spyropoulos *et al.*, 2004) to determine and visualize its predicted transmembrane domain and topology. We also used GPS 3.0 (http://gps.biocuckoo.cn/online.php) to identify potential phosphorylation sites. We then performed a Clustal W sequence alignment using Lasergene MegAlign v. 15 (DNAStar, Madison, WI) to show amino acid conservation among several vertebrate species (**Supplemental Figure S1**).

We used the single nucleotide polymorphism (SNP) database from the National Center for

Biotechnology Information website (NCBI dbSNP; www.ncbi.nlm.nih.gov/snp) to identify specific nucleotide sequence variations within the *TMEM163* gene that results in non-synonymous amino acid substitutions. Based on the predicted secondary structure information we obtained, we selected several SNP-associated non-synonymous amino acid substitutions that we surmised to potentially affect TMEM163's native structure and function. **Supplemental Table S1** provides the list of the SNPs used in the study, namely: Serine to Arginine at position 61 (S61R), Serine to Cysteine at position 95 (S95C), Serine to Proline (S193P), Glycine to Serine at position 229 (G229S), and Glutamate to Lysine at position 286 (E286K). **Supplemental Figure S2** illustrate the location and vertebrate species conservation of the SNPs, respectively.

Cell culture

Human embryonic kidney (HEK)-293 and HeLa cells were purchased from American Type Culture Collection (ATCC; Manassas, VA). We cultured HeLa and HEK-293 cells in Dulbecco's Modified Eagle's Media (DMEM; 4.50 g/L glucose, 0.58 g/L L-glutamine, 0.11 g/L sodium pyruvate; Corning) supplemented with 10% fetal bovine serum (FBS; Thermo Scientific, Waltham, MA), but without antibiotics. The cells were maintained in a humidified standard 37°C incubator supplied with 5% CO_2.

Creation of stable cell lines

We created HeLa cells that stably over-express an empty pmCherry vector control (Takara Bio, Mountain View, CA), a monomeric red fluorescent protein variant (ex = 587 nm, em = 610 nm) (Shaner *et al.*, 2004) and a TMEM163 construct with mCherry fused at the C-terminus region (Cuajungco *et al.*, 2014). Endogenous *TMEM163* transcripts are not detected in HeLa cells (www.proteinatlas.org). The pmCherry N1 vector contains a *Neomycin* resistance gene driven by the SV40 promoter. The TMEM163-mCherry and empty pmCherry vectors were linearized using the *Not I* restriction site and column-purified. The linearized vectors were transfected with TurboFect into a 70% confluent HeLa cells cultured in a 6-well plate. Every two to three days, the DMEM media containing the G418 antibiotic (0.9 mg/mL) was replaced. After two weeks, most of the untransfected cells were dead and the islands of transfected cells exhibiting red fluorescence viewed under an inverted IX-71 Olympus fluorescent microscope (Olympus America, Center Valley, PA) were isolated using cloning cylinders held in place by 1% agarose. The cloning cylinders acted as small wells from which the clonal group could be trypsinized. The dissociated colony cells were re-seeded into a 24-well culture plate. The process was repeated several times to guarantee that untransfected cells were eliminated. We then used fluorescence microscopy to corroborate that each cell line was stably expressing TMEM163 or the plasmid. As additional verification, total RNA was extracted from the stable cell lines using Trizol (Thermo Scientific), and the purified RNA samples were reverse-transcribed to generate cDNAs. The veracity of stable gene expression was established by a standard polymerase chain reaction technique using specific primer sets that anneal only to the mCherry cDNA sequence or the mCherry-tagged *TMEM163* cDNA sequence

RNA Interference (RNAi)

We used a short hairpin RNA (shRNA, 29-mer; OriGene Technologies, Rockville, MD) expression vector that effectively down-regulates TMEM163 expression as we previously reported (Eichelsdoerfer *et al.*, 2010; Cuajungco *et al.*, 2014). We seeded 15,000 HEK-293 cells per well in PDL-treated 96-well culture plate the day before the experiments. Cells in quadruplicate wells were transfected with 2 µg DNA of either TMEM163-KD (knock-down) shRNA or TMEM163-OE (over-expression) construct using TurboFect lipid reagent (Thermo Scientific). Twenty-four hours post-transfection, the cells were washed three times with phosphate-buffered saline (PBS), exposed to low levels of exogenous zinc chloride ($ZnCl_2$, 100 nM) overnight, and washed three times with PBS before the spectrofluorometric assay.

Recombinant DNA constructs and site-directed mutagenesis (SDM) technique

We used a TMEM163-mCherry expression construct (Eichelsdoerfer *et al.*, 2010; Cuajungco *et al.*, 2014) to change a specific amino acid sequence corresponding to the non-synonymous TMEM163 SNPs used in the study (**Supplemental Table S1**). Using the online In-Fusion™ HD (IF) cloning system primer design website (Takara Bio USA, Mountain View, CA), we made primer sets for TMEM163 SNP, ZIP1 (a kind gift of Dr. David J. Eide, University of Wisconsin), and the TMEM163 double aspartate to alanine substitution mutation located at positions 124 and 128 (D124A/D128A) (**Supplemental Table S2**). Note that the double aspartate to alanine mutations were recently reported to decrease zinc binding and inactivate protein function in rodent Tmem163 at positions 123 and 127 (Tmem163-D123A/D127A) (Waberer *et al.*, 2017). We verified the DNA sequence integrity of all expression constructs by commercial sequencing (Retrogen, San Diego, CA) and analyzed

the clone sequences using Lasergene SeqMan v. 15 (DNAStar, Madison, WI).

Spectrofluorometric assays using Fluozin-3 and Newport Green fluorescent dyes

RNAi Expression

After washing out the exogenous zinc, the cells were incubated with 1 μM cell membrane permeable Fluozin-3 acetoxy-methyl ester (AM) fluorescent dye (MP-FZ3; Kd = 15 nM; ex = 494 nm, em = 516 nm; Thermo Scientific). Fluozin-3 is a well-established tool for evaluating changes in relative zinc levels due to its specificity, high dissociation constant, and physiological stability (Zhao *et al.*, 2008). The dye only emits fluorescence when bound to labile or chelatable zinc and the dye remains in the cytoplasm upon ester cleavage of the AM moiety (Gee *et al.*, 2002). We followed the manufacturer's recommendation to incubate MP-FZ3 for 30 minutes inside a 37°C incubator with 5% CO_2. The cells were then washed with PBS three times before performing an end-point assay for intracellular zinc fluorescence as previously described (Eichelsdoerfer *et al.*, 2010; Cuajungco *et al.*, 2014). Un-transfected control cells were included in every experiment (n = 4 independent trials). Background fluorescence was subtracted (blank) from each treatment group to obtain the relative fluorescence unit (RFU). The data were analyzed using Prism 8 (GraphPad, San Diego, CA).

Stable Cell Expression

We optimized the assay for cell membrane impermeable Fluozin-3 (MI-FZ3) and membrane permeable Newport Green dichloro-fluorescein-AM (MP-NG; Kd ~ 1 μM; ex = 505 nm, em = 535 nm; Thermo Scientific) spectrofluorometric assays by identifying the appropriate: (i) cell density; (ii) concentration of exogenous $ZnCl_2$; (iii) concentration of MI-FZ3 or MP-NG; and (iv) buffer types for dye incubation and washing. We also supplemented the incubation and wash buffers with 2 mM Glutamax™ (Thermo Scientific) and 1 mM sodium pyruvate to maintain cell viability throughout the period of experimentation.

We used HeLa cells stably expressing TMEM163-mCherry or pmCherry empty vector control. We seeded 25,000 cells per well in a PDL-treated 96-well plate one day before the experiments. The first six wells of each row were designated as treatment group (zinc exposed), while the remaining six wells in the same row were used as untreated control group (non-exposed). We then exposed the cells to $ZnCl_2$ (10 μM) and zinc pyrithione (1 μM) for 5 minutes and washed three times with HEPES buffer (15 mM HEPES, 100 mM D-glucose, and 150 mM KCl; pH 7.0) using an automated BioTek 405 TS microplate washer (BioTek Instruments, Winooski, VT). A post-washed volume of 100 μL was dispensed and the plate was transferred into the BioTek Cytation V plate reader and each well was dispensed with 100 μL HEPES buffer containing MI-FZ3 dye to a final concentration of 1 μM. We performed kinetic readings for each well every minute for 25 minutes. Average background RFU from non-zinc exposed group (transfected and non-transfected, but not pre-loaded with zinc) was subtracted from RFUs of zinc-exposed group (transfected and non-transfected). Background subtraction minimizes or prevents the confounding effects contributed by native zinc transporters present in cells such as ZNTs and ZIPs, which are both expressed in HeLa and HEK-293 cell lines (Human Protein Atlas, www.proteinatlas.org). Five-minute data point intervals were collected and analyzed using Prism 8.

To further support the MI-FZ3 results, we then performed assays using MP-NG. HeLa cells stably expressing TMEM163 and pmCherry vector control were seeded at 25,000 cells per well in a PDL-treated 96-well plate. The cells were incubated with MP-NG (5 μM) for 20 minutes inside a 37°C incubator with 5% CO_2, washed two times with a standard buffer (10 mM HEPES, 135 mM NaCl, 5 mM KCl, 1 mM $CaCl_2$, 1 mM $MgSO_4$, and 5 mM glucose; pH 7.4), and left at room temperature for another 30 minutes to ensure complete ester cleavage of AM moiety. The treatment group was exposed to $ZnCl_2$ (100 μM) and pyrithione (10 μM) for 20 minutes inside the incubator, washed five times with standard buffer, and each well was dispensed with a final volume of 100 μL standard buffer after the last wash. A kinetic reading for zinc flux was performed every minute for 45 minutes using the BioTek Cytation V plate reader. Background extracellular MI-FZ3 RFU levels (no zinc exposure) were subtracted from the zinc-treated RFU levels. We adapted a previously described protocol (Ohana *et al.*, 2009) to quantify changes in cytoplasmic zinc levels by dividing the RFU timepoint readings with the baseline RFU taken at time zero. Data points from 5-minute interval reads were collected and analyzed using Prism 8.

Transient Cell Expression

To further corroborate the stable expression data and include additional controls, we performed transient transfection of the following constructs: pmCherry empty vector, TMEM163-mCherry, ZIP1-mCherry (a known influx transporter), and TMEM163-D124/D128A-mCherry (a similar double mutation reported to inactivate rodent Tmem163) (Waberer *et al.*, 2017). We seeded HEK-293 cells at 15,000 cells per well on a 96-well culture plate treated with PDL one

day before transfection. The first six wells of each row were designated as treatment group (zinc exposed), while the remaining six wells in the same row were used as untreated control group (non-exposed). We transfected the cells with a standard amount of 150 ng of DNA constructs per well using TurboFect lipid reagent. A standard amount of 200 ng DNA was used per well for the empty vector control to match the efficiency of transfection in cells treated with the expression constructs containing a specific gene. Twenty-four hours post-transfection, the culture medium was aspirated, and each well was dispensed 100 µL of HEPES buffer with zinc (treated) or without zinc (untreated). The treated cells were exposed to $ZnCl_2$ (10 µM) and zinc pyrithione (1 µM) for 5 minutes in a standard humidified 37°C incubator with 5% CO_2. The cells were then washed three times with HEPES buffer using an automated BioTek 405 TS microplate washer to minimize or prevent cells from lifting out of the well surface, and after the final liquid aspiration, each well was dispensed with 100 µL of HEPES buffer containing MI-FZ3 dye to a final concentration of 1 µM. The plate was transferred into the BioTek Cytation V plate reader and each well was assayed (kinetic reading) for zinc flux every minute for 25 minutes. To analyze the raw data, the background RFU values (no zinc exposure) were subtracted from zinc-treated RFU data as described earlier. Five-minute data point intervals were collected and analyzed using Prism 8.

To show that the MI-FZ3 fluorescence signal is directly attributable to zinc, we used the metal chelator N,N,N,N-*tetrakis*-(2-pyridylmethyl)-ethylenediamine (TPEN, 10 µM) in several transient transfection experiments as described earlier by injecting the chelator half-way through the kinetic reading. TPEN is a zinc-specific, high affinity chelator (Kd = 10^{-16} M) that binds chelatable zinc *in vivo* (Cuajungco and Lees, 1996; 1998) or *in vitro* (Zalewski *et al.*, 1993; Ahn *et al.*, 1998). One-minute interval reads were graphed using Prism 8.

To evaluate the effects of each non-synonymous SNP on TMEM163 function, we seeded HEK-293 at 15,000 cells per well in a PDL-treated 96-well plate the day before the experiment. Similar to the above approach for MI-FZ3, the first six wells were designated as zinc-treated group, while the last six wells were used as non-zinc treated group. We used TurboFect to transfect the cells with the following non-synonymous SNP-associated constructs (150 ng DNA): TMEM163-S61R-mCherry, TMEM163-S95C-mCherry, TMEM163-S193P-mCherry, TMEM163-G229S-mCherry, and TMEM163-E286K-mCherry. Twenty-four hours post transfection, the cells were pre-loaded with $ZnCl_2$ (10 µM) and zinc pyrithione (1 µM) for 20 minutes, washed twice with HEPES buffer, and transferred to the plate reader for kinetic reading after injection of the MI-FZ3 dye (1 µM). A kinetic reading for zinc flux was performed every minute for 25 minutes using the BioTek Cytation V plate reader and the background RFU values were subtracted from the zinc-treated RFU values. Data points every 5 minutes were collected for analysis using Prism 8.

Cell viability assay

To investigate whether the SNPs and the TMEM163-D124A/D128A constructs affect cell health, we seeded 15,000 HEK-293 cells in a PDL-treated 96-well plate. Cells in quadruplicate wells were transfected with wild-type TMEM163 (TMEM163-WT), TMEM163-D124A/D128A, TMEM163-S61R, TMEM163-S193P, TMEM163-E286K, and pmCherry empty vector control. We then assessed cell viability of treated and control cells 48 hours post-transfection using the CellTiter Glo 2.0 luciferase assay kit (Promega, Madison, WI) according to the manufacturer's protocol. The data were normalized using un-transfected control cells and represented as percentage of control (n = 5 independent trials).

Immunocytochemistry (ICC) and Fluorescence microscopy analysis

HEK-293 cells were seeded in sterile coverslips at approximately 30% confluency one day before transfection of specific expression constructs used in the study. The mammalian expression constructs either contained a fluorescent (mCherry; Takara Bio) protein tag or peptide tag (Myc-DDK; OriGene Technologies). Images of the mCherry-tagged transfected cells were taken 24 hours post-transfection. This approach also allowed us to check for transfection efficiency and cell viability. For mCherry-tagged constructs, fluorescence imaging was done using an inverted Olympus IX-71 fluorescence microscope. Monochromatic RGB images of cells were captured using the CellSens software version 1.18 (Olympus), and we then used Adobe Photoshop CC 2017 (Adobe Systems, San Jose, CA) to show the images in red color to correspond with the mCherry fluorescence.

For Myc-DDK-tagged constructs, the cells were fixed with 4% paraformaldehyde for 15 minutes, washed three times with PBT1 buffer (1X PBS, 1% Triton-X 100, 0.1% BSA, 5% heat-inactivated goat serum) and incubated with primary antibody (1:1000 anti-DDK monoclonal 4C5; OriGene Technologies) in PBT1 at 4°C overnight. The cells were washed with PBT2 buffer (1X PBS, 1% Triton-X 100, 0.1% BSA) three times, and then incubated with secondary antibody (1:500 anti-mouse Alexa Fluor-488; ex = 490 nm, em = 525 nm; Thermo Scientific) in PBT2 for 2

hours at 4°C. The cells were then washed two times with 1X PBS. Each coverslip was mounted on a slide, treated with Prolong Gold anti-fade reagent (Thermo Scientific) and the edge of the coverslip was sealed with clear nail polish. Monochrome images were taken using an upright Olympus BX51 fluorescence microscope and processed using Adobe Photoshop to change the monochrome images to green color as represented by Alexa-488 fluorescence.

Statistical Analysis

All numerical data were graphed and analyzed for statistical significance using Prism 8 software. We used Student's *t*-test (paired, two-tailed) to determine statistical significance of experiments using stable cells expressing TMEM163 and pmCherry vector control. Data obtained from other spectrofluorometric experiments were analyzed using one-way analysis of variance (ANOVA) with repeated measures and Tukey's multiple comparisons *post-hoc* test. The significance level was set at $p < 0.05$. Unless specified, all data are represented as mean ± SEM with at least three independent trials.

RESULTS

TMEM163 is a zinc effluxer

TMEM163 has a predicted six transmembrane domain (TMD) and is highly conserved among the vertebrate species we analyzed (**Supplemental Figure S1**). RNAi of TMEM163 in HEK-293 cells produced a substantial increase in intracellular MP-FZ3 fluorescence, while over-expression of TMEM163 exhibited an opposite effect (**Supplemental Figure S3**), which was consistent with our previous observation (Cuajungco *et al.*, 2014). This result gave us *a priori* information that TMEM163 may be transporting zinc out of the cells. We used two different types of human cell lines and two heterologous expression systems (i.e. stable and transient), in order to show the reproducibility and specificity of our spectrofluorometric data. To first show that TMEM163 effluxes zinc, we created HeLa cells stably expressing TMEM163 and analyzed zinc flux upon zinc exposure using either MI-FZ3 or MP-NG. For MI-FZ3 assay, we found a substantial increase in extracellular fluorescence among TMEM163-expressing cells in comparison to the pmCherry control (**Fig.1A**). For MP-NG, a substantial reduction of intracellular MP-NG fluorescence was observed from cells expressing TMEM163 when compared to the pmCherry control (**Fig. 1B**).

Loss-of-function mutation negatively affects TMEM163 function but not membrane localization

We then looked at the effects of transient heterologous expression of TMEM163 in HEK-293 cells. In addition to pmCherry empty vector control, we used ZIP1 (a zinc influx transporter), and the double aspartate to alanine substitutions, TMEM163-D124A/128A. These alanine mutations are equivalent to the previously reported inactive rodent Tmem163-D123A/D127A (Waberer *et al.*, 2017). We observed a discernable increase of MI-FZ3 fluorescence in the milieu of cells transiently expressing TMEM163, but not pmCherry empty vector control, ZIP1, and TMEM163-D124A/D128A (**Fig. 2A**). Analysis of variance (ANOVA) with repeated measures and *post-hoc* analysis using Dunnett's multiple comparisons test showed significant differences between TMEM163 and: i) TMEM163-D124A/D128A ($p < 0.0001$); ii) ZIP1 ($p < 0.0001$); and iii) pmCherry ($p = 0.002$). To demonstrate that the MI-FZ3 fluorescence signal is contributed by zinc extrusion in the cellular environment, we performed additional experiments in which we injected TPEN during the kinetic measurement. TPEN is a cell membrane permeant chelator that binds avidly to zinc (Cuajungco and Lees, 1996; 1998). We found that TPEN completely abrogated the MI-FZ3 fluorescence signal (**Supplemental Fig. S4**).

We wanted to ensure that the marked difference in zinc efflux activity between wild-type TMEM163 and TMEM163-D124A/D128A was not caused by either transfection or cell expression issues. We therefore took fluorescent images of the cells for evidence of transfection before performing the assays. We performed fluorescence microscopy studies to determine the expression profiles of all four constructs. The results showed that TMEM163 is localized within the plasma membrane (PM) and intracellular membrane compartments (MC) (**Fig. 2B**), which confirmed our previous observation (Cuajungco *et al.*, 2014). Interestingly, the subcellular localization of TMEM163-D124A/D128A appeared to be similar to the wild-type protein where it is detected in both the PM and MC. ZIP1 expression was detected in the PM and more prominently within MC, which happens to be consistent with previous reports (Gaither and Eide, 2001; Wang *et al.*, 2004). As expected, the pmCherry empty vector was mainly observed in the cytoplasm.

Missense mutations in conserved amino acid residues negatively affects zinc efflux

Based on the negative effect of double mutation located within the predicted TMD2 of TMEM163, we hypothesized that a single point mutation within certain key amino acid residues could potentially disrupt, if not abolish, its normal efflux function. To avoid simply selecting amino acids based on information from

prediction software tools, we chose to look at specific non-synonymous SNPs that have been identified within the *TMEM163* gene using NCBI's dbSNP database (**Supplemental Table S1**). We picked four non-synonymous SNPs of serine (i.e. S61R, S95C, and S193P) and glutamate (i.e. E286K) residues due to their species conservation, position within the predicted secondary structure, and possible target for post-translational modification (**Supplemental Figs. S1 and S2**). For example, S61, S95, and S193 are potential phosphorylation sites while E286 is a negatively charged residue. We transiently expressed the non-synonymous SNP constructs in HEK-293 cells along with the wild-type TMEM163 and pmCherry empty vector. For this set of experiments, we exposed the cells to zinc and pyrithione for an extra 15 minutes, in order to gauge whether the amino acid substitution could also affect cell health. We found that the cells expressing the SNP constructs showed significant reductions in extracellular MI-FZ3 fluorescence signal when compared with wild-type TMEM163 (**Fig. 3A**). ANOVA with repeated measures and *post-hoc* analysis using Dunnett's multiple comparisons test showed significant differences between wild-type TMEM163 and: i) S61R (p = 0.001); ii) S95C (p = 0.04); S193P (p = 0.0004); and iii) E286K (p = 0.0005). The MI-FZ3 fluorescence signals coming from cells expressing S61R, S95C, and S193P constructs were very similar to that of cells expressing the pmCherry empty vector control. Note, however, that the cells expressing the E286K construct displayed the lowest efflux activity, which was well below the fluorescence obtained from pmCherry empty vector control (**Fig. 3A**).

Most of the mutated TMEM163 alleles localize to cell membrane

Similar to our earlier experimental approach, we captured fluorescence images of the cells expressing the SNPs to determine transfection efficiency and expression profile before we performed each MI-FZ3 assay. Fluorescence microscopy analyses of SNP constructs tagged with mCherry fluorescent protein or Myc-DDK peptide (**Fig. 3B**) showed a very similar expression pattern to the wild-type TMEM163 protein despite differences in efflux activity. It is worth noting that the S193P expression profile with mCherry tag appeared exclusively within the cytoplasm, which was very similar to cells expressing the empty pmCherry vector control. On the other hand, S193P with Myc-DDK tag was mainly localized within MC but was also detected in PM. To provide additional confirmation that the decline of zinc efflux activity among non-synonymous SNPs and D124A/D128A constructs was not caused by diminished cell health, we performed cell viability assays and found no indication of cytotoxicity in these cells (**Fig. 4**). Although the cells expressing the S95C construct exhibited relatively lower viability, the values were not significant when compared to wild-type TMEM163 and other treatments. Overall, all the experimental results provide compelling evidence that TMEM163 is a zinc effluxer.

DISCUSSION

Our investigations on the function of TMEM163 using two different human cell lines and several independent techniques ultimately revealed that TMEM163 serves to transport zinc out of the cell or the cytoplasm.

Our interests on human TMEM163 protein stemmed from our previous discovery that it is an interaction partner of the Transient Receptor Potential Mucolipin-1 (TRPML1) protein (Cuajungco *et al.*, 2014). Recently, it was shown that rodent Tmem163 interacts with itself and forms a functional dimer (Waberer *et al.*, 2017). Despite being predicted as an efflux transporter, earlier reports on rodent Tmem163 (Barth *et al.*, 2011; Waberer *et al.*, 2017) and our work on human TMEM163 (Cuajungco and Kiselyov, 2017) have suggested that the protein might be operating as an influx transporter. A case in point, it was reported that PC12 cells that heterologously express rodent Tmem163 displayed a noticeable rise in MP-FZ3 fluorescence within the cytoplasm upon exposure to zinc (Barth *et al.*, 2011). This report suggested that Tmem163 transports extracellular zinc inside the cells (Barth *et al.*, 2011). In our preliminary study, TMEM163-expressing HEK-293 cells incubated with zinc produce a discernible up-regulation of MT-1A transcripts when compared with control cells after twenty-four hours (Cuajungco and Kiselyov, 2017), which suggests that TMEM163 could be an influxer. In contrast, when we knocked down TMEM163 expression in HEK-293 cells using RNAi, the fluorescence intensity of MP-FZ3 dye inside the cells remains considerably higher than control cells (**Supplemental Fig. S3**) (Cuajungco *et al.*, 2014). After carefully re-analyzing these contradictory observations, we concluded that TMEM163 may actually be bringing zinc out of the cells in response to high cytosolic zinc levels. We believe that endogenous zinc transporters (ZNTs and ZIPs) confounded our previous interpretation of increased MT-1A expression upon TMEM163 expression. It is possible that the over-expression of TMEM163 increased zinc efflux, but then induced a compensatory zinc uptake through native zinc influxers, and subsequently increased the expression of MT-1A. Indeed, transcripts of several zinc influx *SLC39* (*ZIP*) genes (e.g. ZIP1, ZIP3, ZIP6-

ZIP10, ZIP13, and ZIP14) are detected in HEK-293 and HeLa cells (www.proteinatlas.org). Meanwhile, transcripts of some *SLC30* (*ZNT*) genes are also detected in HEK-293 cells (e.g. ZNT5 and ZNT6) and HeLa cells (e.g. ZNT1, ZNT5, and ZNT6) (www.proteinatlas.org). Waberer and colleagues (2017) circumvented the potential confounding effects of native zinc influx and efflux proteins by using artificial liposomes. In their report, they purified rodent Tmem163 proteins and inserted them into lipid nanodiscs. This approach allowed them to show that Tmem163 binds to and transports zinc as evidenced by an increase in cell membrane permeant Fluozin-1 fluorescence inside the liposomes (Waberer *et al.*, 2017). While this elegant technique provided evidence for Tmem163-mediated zinc transport, it did not show whether the protein is an influxer or effluxer in living cells. Despite challenges in utilizing human cell lines, we successfully showed that TMEM163 extrudes zinc out of the cytoplasm upon intracellular zinc elevation.

The dramatic negative response of TMEM163-D124A/D128A mutation on zinc efflux in comparison to ZIP1 and pmCherry vector control was unexpected, because if these mutations actually inactive the protein as has been reported for rodent Tmem163-D123A/D127A (Waberer *et al.*, 2017), then we would expect the fluorescence signal to be similar in magnitude to that of pmCherry empty vector control. Our data show that the depressed efflux activity of the double mutation is not due to mis-localization and/or cell toxicity as demonstrated by fluorescence imaging and viability assays, respectively. It is conceivable that the TMEM163-D124A/D128A monomer acts in a dominant negative manner upon dimerization with native TMEM163 monomers present in HEK-293 cells. We also cannot rule out the prospect that TMEM163-D124A/D128A may interact and induce a dominant negative effect on native zinc transporters present in cells (e.g. ZNTs), since various zinc efflux transporters have been reported to form heterodimers (Fukunaka *et al.*, 2009; Salazar *et al.*, 2009; Lasry *et al.*, 2014; Golan *et al.*, 2015). It would be interesting to find out in future studies if TMEM163-D124A/D128A's ability to dimerize with wild-type TMEM163 or potential to interact with other zinc transporters is the main reason for its dominant negative effect on efflux activity. Nevertheless, the negative effect of the double aspartate mutation on the role of TMEM163 is further evidence that it is a zinc efflux transporter.

For experiments studying the consequence of non-synonymous SNPs in HEK-293 cells, we found that the amino acid substitution in three serine residues (S61R, S95C, and S193P) or in one glutamate residue (E286K) completely altered TMEM163's role in extruding cytoplasmic zinc. Serine residues are potential post-translational modification (PTM) target where it can be phosphorylated. Prediction-based PTM analysis of TMEM163's amino acid sequence using GPS 3.0 (http://gps.biocuckoo.cn/index.php) (Xue *et al.*, 2011) shows potential kinases targeting positions S61, S95, and S193. It would be interesting to determine in future investigation if these sites are truly phosphorylated and which protein kinases are involved. Meanwhile, the apparent mis-localization of S193P when tagged with a fluorescent protein, but not with dual Myc-DDK peptide, suggests that the proline substitution within the predicted TMD4 may have kinked the alpha-helical structure (Grimm *et al.*, 2007; Cuajungco and Samie, 2008) such that it induced a conformational change due to the presence of the mCherry fluorescent protein tag (mCherry has a molecular mass of 26.7 kDa (Shaner *et al.*, 2004)). Meanwhile, it is not clear why the zinc efflux activity of E286K is dramatically reduced, which is virtually comparable to D124A/D128A mutant. It is plausible that the change from a negatively-charged glutamate to a positively-charged lysine residue altered the protein's structure, which then created a dominant negative mutant like that of the D124A/D128A mutant. Future studies on TMEM163 structure and function could explain the probable dominant negative effect of site-specific mutations within the protein. Nevertheless, the reduction of zinc efflux activity observed from these non-synonymous SNPs provided additional support that TMEM163 is an effluxer. Figure 5 illustrates a summary of the current findings.

In conclusion, our findings reveal that TMEM163 plays a key role in cellular zinc homeostasis by extruding cytoplasmic zinc ions outside of the cells. Future investigations on the importance of TMEM163 in select human tissues or organs, and its potential contributions to normal and pathological states are therefore warranted.

ACKNOWLEDGMENTS

We are very grateful to Lauren Rosas, Joshua Silva, Cathleen Nguyen, and Quinlan Cantrell for their technical support. We also thank Dr. Sean Murray (CSU Northridge) for reading and critiquing the manuscript. MPC is funded by the National Institutes of Health (NIH) NINDS AREA grant R15 NS101594. VS is supported by the NIH NIGMS MARC U*STAR T34 GM008612 training grant. The content of this paper is solely the responsibility of the authors and does not necessarily represent the official views of the NIH.

CONFLICTS OF INTEREST

The authors declare no conflicts of interest with the contents of this article.

AUTHOR CONTRIBUTIONS

MPC conceived and designed the study, project administration, data analysis and interpretation, wrote original manuscript. VBS performed experiments, analyzed data, and edited the manuscript. SA performed experiments including assay optimization, analyzed data, and edited the manuscript. All authors read and approved the final manuscript.

REFERENCES

Ahn, Y.H., Kim, Y.H., Hong, S.H., Koh, J.Y. (1998) Depletion of intracellular zinc induces protein synthesis-dependent neuronal apoptosis in mouse cortical culture. Exp Neurol 154, 47-56.

Aiken, S.P., Horn, N.M., Saunders, N.R. (1992) Effects of histidine on tissue zinc distribution in rats. BioMetals 5, 235-243.

Aydemir, T.B., Kim, M.H., Kim, J., Colon-Perez, L.M., Banan, G., Mareci, T.H., Febo, M., Cousins, R.J. (2017) Metal Transporter Zip14 (Slc39a14) Deletion in Mice Increases Manganese Deposition and Produces Neurotoxic Signatures and Diminished Motor Activity. J Neurosci 37, 5996-6006.

Barth, J., Zimmermann, H., Volknandt, W. (2011) SV31 is a Zn2+-binding synaptic vesicle protein. J Neurochem 118, 558-570.

Beyer, N., Coulson, D.T., Heggarty, S., Ravid, R., Irvine, G.B., Hellemans, J., Johnston, J.A. (2009) ZnT3 mRNA levels are reduced in Alzheimer's disease post-mortem brain. Mol Neurodegener 4, 53.

Bosomworth, H.J., Adlard, P.A., Ford, D., Valentine, R.A. (2013) Altered expression of ZnT10 in Alzheimer's disease brain. PLoS One 8, e65475.

Burre, J., Zimmermann, H., Volknandt, W. (2007) Identification and characterization of SV31, a novel synaptic vesicle membrane protein and potential transporter. J Neurochem 103, 276-287.

Choi, B.Y., Kim, I.Y., Kim, J.H., Kho, A.R., Lee, S.H., Lee, B.E., Sohn, M., Koh, J.Y., Suh, S.W. (2016) Zinc transporter 3 (ZnT3) gene deletion reduces spinal cord white matter damage and motor deficits in a murine MOG-induced multiple sclerosis model. Neurobiol Dis 94, 205-212.

Choi, D.W., Yokoyama, M., Koh, J. (1988) Zinc neurotoxicity in cortical cell culture. Neuroscience 24, 67-79.

Colvin, R.A., Holmes, W.R., Fontaine, C.P., Maret, W. (2010) Cytosolic zinc buffering and muffling: their role in intracellular zinc homeostasis. Metallomics 2, 306-317.

Cuajungco, M.P., Basilio, L.C., Silva, J., Hart, T., Tringali, J., Chen, C.C., Biel, M., Grimm, C. (2014) Cellular zinc levels are modulated by TRPML1-TMEM163 interaction. Traffic 15, 1247-1265.

Cuajungco, M.P., Goldstein, L.E., Nunomura, A., Smith, M.A., Lim, J.T., Atwood, C.S., Huang, X., Farrag, Y.W., Perry, G., Bush, A.I. (2000) Evidence that the beta-amyloid plaques of Alzheimer's disease represent the redox-silencing and entombment of abeta by zinc. J Biol Chem 275, 19439-19442.

Cuajungco, M.P., Kiselyov, K. (2017) The mucolipin-1 (TRPML1) ion channel, transmembrane-163 (TMEM163) protein, and lysosomal zinc handling. Front Biosci (Landmark Ed) 22, 1330-1343.

Cuajungco, M.P., Lees, G.J. (1996) Prevention of zinc neurotoxicity in vivo by N,N,N',N'-tetrakis (2-pyridylmethyl) ethylene-diamine (TPEN). Neuroreport 7, 1301-1304.

Cuajungco, M.P., Lees, G.J. (1997a) Zinc and Alzheimer's disease: is there a direct link? Brain Res Brain Res Rev 23, 219-236.

Cuajungco, M.P., Lees, G.J. (1997b) Zinc metabolism in the brain: relevance to human neurodegenerative disorders. Neurobiol Dis 4, 137-169.

Cuajungco, M.P., Lees, G.J. (1998) Diverse effects of metal chelating agents on the neuronal cytotoxicity of zinc in the hippocampus. Brain Res 799, 97-107.

Cuajungco, M.P., Samie, M.A. (2008) The varitint-waddler mouse phenotypes and the TRPML3 ion channel mutation: cause and consequence. Pflugers Arch 457, 463-473.

Danscher, G., Jensen, K.B., Frederickson, C.J., Kemp, K., Andreasen, A., Juhl, S., Stoltenberg, M., Ravid, R. (1997) Increased amount of zinc in the hippocampus and amygdala of Alzheimer's diseased brains: a proton-induced X-ray emission spectroscopic analysis of cryostat sections from autopsy material. J Neurosci Methods 76, 53-59.

Eichelsdoerfer, J.L., Evans, J.A., Slaugenhaupt, S.A., Cuajungco, M.P. (2010) Zinc dyshomeostasis is linked with the loss of mucolipidosis IV-associated TRPML1 ion channel. J Biol Chem 285, 34304-34308.

Eide, D.J. (2006) Zinc transporters and the cellular trafficking of zinc. Biochim Biophys Acta 1763, 711-722.

Fukunaka, A., Suzuki, T., Kurokawa, Y., Yamazaki, T., Fujiwara, N., Ishihara, K., Migaki, H., Okumura, K., Masuda, S., Yamaguchi-Iwai, Y., Nagao, M., Kambe, T. (2009) Demonstration and characterization of the heterodimerization of ZnT5 and ZnT6 in the early secretory pathway. J Biol Chem 284, 30798-30806.

Gaither, L.A., Eide, D.J. (2001) The human ZIP1 transporter mediates zinc uptake in human K562 erythroleukemia cells. J Biol Chem 276, 22258-22264.

Gee, K.R., Zhou, Z.L., Qian, W.J., Kennedy, R. (2002) Detection and imaging of zinc secretion from pancreatic beta-cells using a new fluorescent zinc indicator. J Am Chem Soc 124, 776-778.

Golan, Y., Berman, B., Assaraf, Y.G. (2015) Heterodimerization, altered subcellular localization, and function of multiple zinc transporters in viable cells using bimolecular fluorescence complementation. J Biol Chem 290, 9050-9063.

Grimm, C., Cuajungco, M.P., van Aken, A.F., Schnee, M., Jors, S., Kros, C.J., Ricci, A.J., Heller, S. (2007) A helix-breaking mutation in TRPML3 leads to constitutive activity underlying deafness in the varitint-waddler mouse. Proc Natl Acad Sci U S A 104, 19583-19588.

Hofmann, K., Stoffel, W. (1993) TMbase - A database of membrane spanning proteins segments. Biol Chem 374, 166.

Horn, N.M., Thomas, A.L., Tompkins, J.D. (1995) The effect of histidine and cysteine on zinc influx into rat and human erythrocytes. J Physiol 489 (Pt 1), 73-80.

Itoh, M., Ebadi, M., Swanson, S. (1983) The presence of zinc-binding proteins in brain. J Neurochem 41, 823-829.

Kambe, T., Hashimoto, A., Fujimoto, S. (2014) Current understanding of ZIP and ZnT zinc transporters in human health and diseases. Cell Mol Life Sci 71, 3281-3295.

Kaneko, M., Noguchi, T., Ikegami, S., Sakurai, T., Kakita, A., Toyoshima, Y., Kambe, T., Yamada, M., Inden, M., Hara, H., Oyanagi, K., Inuzuka, T., Takahashi, H., Hozumi, I. (2015) Zinc transporters ZnT3 and ZnT6 are downregulated in the spinal cords of patients with sporadic amyotrophic lateral sclerosis. J Neurosci Res 93, 370-379.

Kim, J., Kim, T.Y., Hwang, J.J., Lee, J.Y., Shin, J.H., Gwag, B.J., Koh, J.Y. (2009) Accumulation of labile zinc in neurons and astrocytes in the spinal cords of G93A SOD-1 transgenic mice. Neurobiol Dis 34, 221-229.

Koh, J.Y., Choi, D.W. (1994) Zinc toxicity on cultured cortical neurons: involvement of N-methyl-D-aspartate receptors. Neuroscience 60, 1049-1057.

Koh, J.Y., Suh, S.W., Gwag, B.J., He, Y.Y., Hsu, C.Y., Choi, D.W. (1996) The role of zinc in selective neuronal death after transient global cerebral ischemia. Science 272, 1013-1016.

Kukic, I., Kelleher, S.L., Kiselyov, K. (2014) Zinc efflux through lysosomal exocytosis prevents zinc-induced toxicity. J Cell Sci 127, 3094-3103.

Lasry, I., Golan, Y., Berman, B., Amram, N., Glaser, F., Assaraf, Y.G. (2014) In situ dimerization of multiple wild type and mutant zinc transporters in live cells using bimolecular fluorescence complementation. J Biol Chem 289, 7275-7292.

Medvedeva, Y.V., Lin, B., Shuttleworth, C.W., Weiss, J.H. (2009) Intracellular Zn2+ accumulation contributes to synaptic failure, mitochondrial depolarization, and cell death in an acute slice oxygen-glucose deprivation model of ischemia. J Neurosci 29, 1105-1114.

Ohana, E., Hoch, E., Keasar, C., Kambe, T., Yifrach, O., Hershfinkel, M., Sekler, I. (2009) Identification of the Zn2+ binding site and mode of operation of a mammalian Zn2+ transporter. J Biol Chem 284, 17677-17686.

Salazar, G., Falcon-Perez, J.M., Harrison, R., Faundez, V. (2009) SLC30A3 (ZnT3) oligomerization by dityrosine bonds regulates its subcellular localization and metal transport capacity. PLoS One 4, e5896.

Scarr, E., Udawela, M., Greenough, M.A., Neo, J., Suk Seo, M., Money, T.T., Upadhyay, A., Bush, A.I., Everall, I.P., Thomas, E.A., Dean, B. (2016) Increased cortical expression of the zinc transporter SLC39A12 suggests a breakdown in zinc cellular homeostasis as part of the pathophysiology of schizophrenia. NPJ Schizophr 2, 16002.

Shaner, N.C., Campbell, R.E., Steinbach, P.A., Giepmans, B.N., Palmer, A.E., Tsien, R.Y. (2004) Improved monomeric red, orange and yellow fluorescent proteins derived from Discosoma sp. red fluorescent protein. Nat Biotechnol 22, 1567-1572.

Smailhodzic, D., van Asten, F., Blom, A.M., Mohlin, F.C., den Hollander, A.I., van de Ven, J.P., van Huet, R.A., Groenewoud, J.M., Tian, Y., Berendschot, T.T., Lechanteur, Y.T., Fauser, S., de Bruijn, C., Daha, M.R., van der Wilt, G.J., Hoyng, C.B., Klevering, B.J. (2014) Zinc supplementation inhibits complement activation in age-related macular degeneration. PLoS One 9, e112682.

Spyropoulos, I.C., Liakopoulos, T.D., Bagos, P.G., Hamodrakas, S.J. (2004) TMRPres2D: high quality visual representation of transmembrane protein models. Bioinformatics 20, 3258-3260.

Waberer, L., Henrich, E., Peetz, O., Morgner, N., Dotsch, V., Bernhard, F., Volknandt, W. (2017) The synaptic vesicle protein SV31 assembles into a dimer and transports Zn(2). J Neurochem 140, 280-293.

Wang, F., Dufner-Beattie, J., Kim, B.E., Petris, M.J., Andrews, G., Eide, D.J. (2004) Zinc-stimulated endocytosis controls activity of the mouse ZIP1 and ZIP3 zinc uptake transporters. J Biol Chem 279, 24631-24639.

Xue, Y., Liu, Z., Cao, J., Ma, Q., Gao, X., Wang, Q., Jin, C., Zhou, Y., Wen, L., Ren, J. (2011) GPS 2.1: enhanced prediction of kinase-specific phosphorylation sites with an algorithm of motif length selection. Protein Eng Des Sel 24, 255-260.

Yoo, M.H., Lee, J.Y., Lee, S.E., Koh, J.Y., Yoon, Y.H. (2004) Protection by pyruvate of rat retinal cells against zinc toxicity in vitro, and pressure-induced ischemia in vivo. Invest Ophthalmol Vis Sci 45, 1523-1530.

Zalewski, P.D., Forbes, I.J., Betts, W.H. (1993) Correlation of apoptosis with change in intracellular labile Zn(II) using zinquin [(2-methyl-8-p-toluenesulphonamido-6-quinolyloxy)acetic acid], a new specific fluorescent probe for Zn(II). Biochem J 296 (Pt 2), 403-408.

Zhao, J., Bertoglio, B.A., Gee, K.R., Kay, A.R. (2008) The zinc indicator FluoZin-3 is not perturbed significantly by physiological levels of calcium or magnesium. Cell Calcium 44, 422-426.

FIGURE LEGENDS

Figure 1. Spectrofluorometric assays of HeLa cells stably expressing TMEM163 and pmCherry vector. A) Cell membrane impermeant Fluozin-3 fluorescence analysis revealed a significant increase in extracellular RFU levels in the milieu of cells expressing TMEM163-mCherry upon exposure to zinc. Data are represented as mean ± SEM (****$p < 0.0001$, Student's *t*-test, unpaired, two-tailed; n = 5 independent trials). **B**) Cell membrane permeant NG fluorescence analysis revealed a significant decrease in intracellular RFU levels of cells expressing TMEM163-mCherry upon exposure to zinc when compared with cells expressing the pmCherry vector control. Data are represented as mean ± SEM of each kinetic time point analyzed (*$p = 0.01$; Student's *t*-test, unpaired, two-tailed; n = 6 independent trials).

Figure 2. Spectrofluorometric assay and fluorescence microscopy of HEK-293 cells transiently expressing wild-type TMEM163, TMEM163-D124A/128A mutant, ZIP1, and pmCherry empty vector control. A) Cell membrane impermeant Fluozin-3 fluorescence analysis reveals a significant increase in extracellular fluorescence upon expression of TMEM163 protein when compared with controls. Data are represented as mean ± SEM of each kinetic time point analyzed (**$p = 0.002$, ****$p < 0.0001$; Tukey's multiple comparisons *post-hoc* test; n ≥ 5 independent trials). **B**) Representative fluorescent micrographs showing subcellular distribution of pmCherry (mCh) empty vector, TMEM163-mCherry, ZIP1-mCherry, and TMEM163-D124A/D128A-mCherry. TMEM163 and TMEM163-D124A/D128A localize within the plasma membrane and membrane compartments (*arrowhead*). ZIP1 is also detected within the plasma membrane and intracellular membrane compartment (*arrowhead*). The pmCherry vector exclusively localizes in the cytoplasm (*arrow*). Scale bar: 50 µm.

Figure 3. Spectrofluorometric assay and fluorescence microscopy of HEK-293 cells transiently expressing wild-type TMEM163 and non-synonymous SNPs: S61R, S95C, S193P, and E286K. A) Cell membrane impermeant Fluozin-3 fluorescence analysis reveals a significant increase in extracellular fluorescence upon expression of TMEM163 protein. Non-synonymous SNPs negatively affect the efflux function of TMEM163, particularly the E286K clone. Data are represented as mean ± SEM of each kinetic time point analyzed (*$p = 0.04$, **$p = 0.004$, ***$p = 0.0004$; Tukey's multiple comparisons *post-hoc* test; n ≥ 4 independent trials). **B**) Representative fluorescent micrographs of expression constructs with mCherry (mCh) fluorescent protein tag (*top panel*) and Myc-DDK peptide tag probed with Alexa Fluor-488 (A488) (*bottom panel*). TMEM163-S61R, TMEM163-S95C, and TMEM163-E286K exhibit localization within the plasma membrane and intracellular membrane compartment (*arrowhead*), while TMEM163-S193P shows mostly cytoplasmic and compartmental localization (*arrow*). Scale bar: 50 µm.

Figure 4. Cell viability of HEK-293 cells expressing wild-type TMEM163, MEM163-D124A/D128A mutant, and non-synonymous SNPs: S61R, S95C, S193P, and E286K. The mammalian expression construct contains the mCherry fluorescent protein tag. Both the TMEM163 mutant and SNPs do not significantly affect cell survival when compared to cells expressing the wild-type TMEM163 construct. Note, however, that cells expressing the S95C construct appear to have slight cytotoxicity in comparison with the other expression constructs. Data are represented as mean ± SEM of % control (n ≥ 4 independent trials).

Figure 5. Schematic diagram summarizing the main observations on the zinc efflux function of TMEM163. Heterologous expression of the wild-type TMEM163 results in cytoplasmic zinc extrusion in the presence of high zinc levels inside the cells. Expression of the non-

synonymous SNPs S61R, S95C, and S193P produces marked reduction of efflux activity when compared with wild-type TMEM163. S193P appears to be mostly expressed in the cytoplasm and MC, while the others are found in the PM and MC. The non-synonymous SNP E286K has the lowest efflux activity in comparison to other SNPs and wild-type TMEM163. Similar to E283K, the D124A/D128A double mutant has comparably lowest efflux activity relative to the wild-type TMEM163 and other SNPs. The rodent Tmem163-equivalent D123A/D127A has been reported to be inactive and unable to bind zinc in a cell-free system (Waberer *et al.*, 2017). PM, plasma membrane; MC, membrane compartments.

Fig. 1

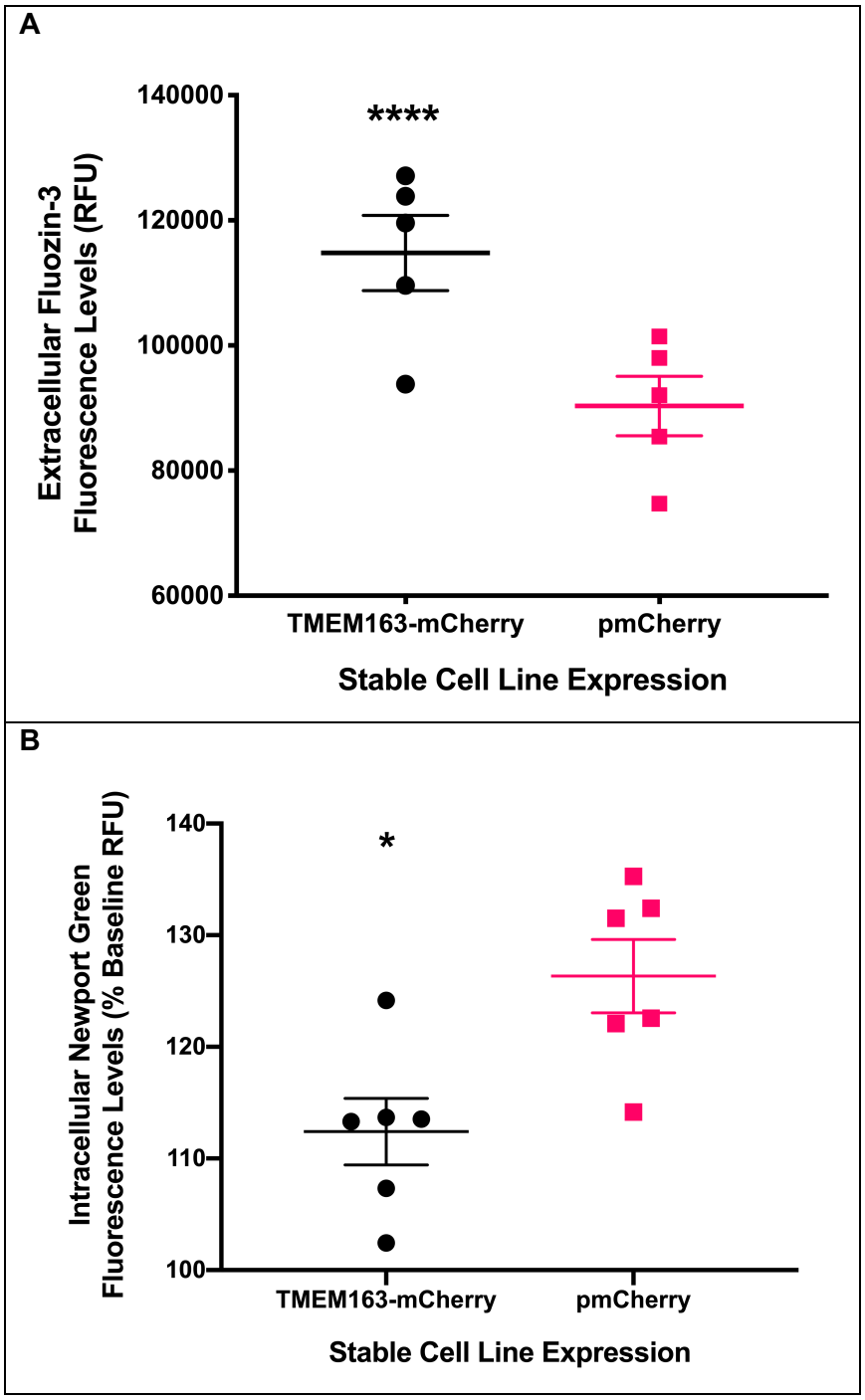
A
Extracellular Fluozin-3
Fluorescence Levels (RFU)
140000
120000
100000
80000
60000
****
TMEM163-mCherry
pmCherry
Stable Cell Line Expression
B
Intracellular Newport Green
Fluorescence Levels (% Baseline RFU)
140
130
120
110
100
*
TMEM163-mCherry
pmCherry
Stable Cell Line Expression

Fig. 2

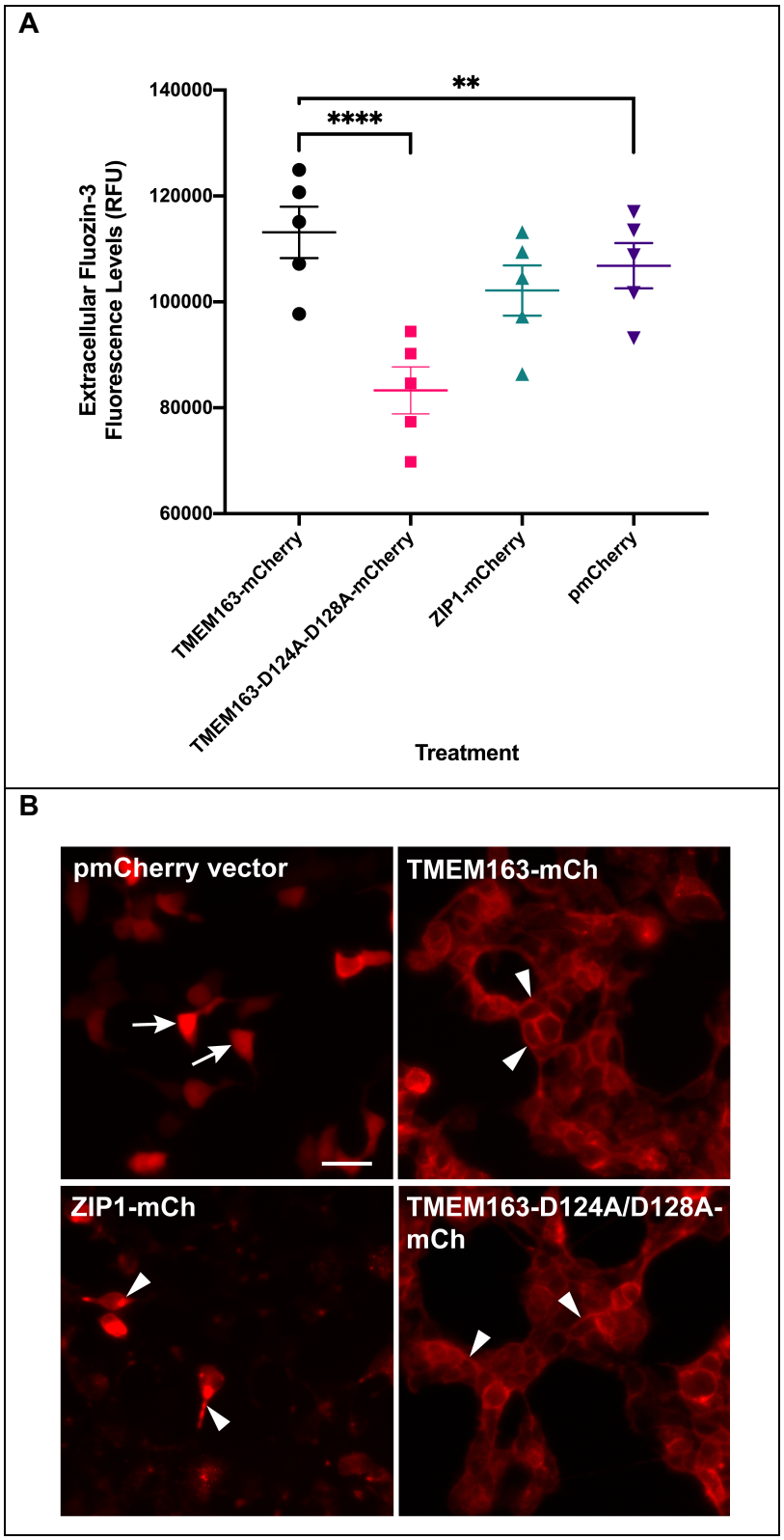
A
140000
120000
100000
80000
60000
Extracellular Fluozin-3 Fluorescence Levels (RFU)
****
**
TMEM163-mCherry
TMEM163-D124A-D128A-mCherry
ZIP1-mCherry
pmCherry
Treatment
B
pmCherry vector
TMEM163-mCh
ZIP1-mCh
TMEM163-D124A/D128A-mCh

Fig. 3

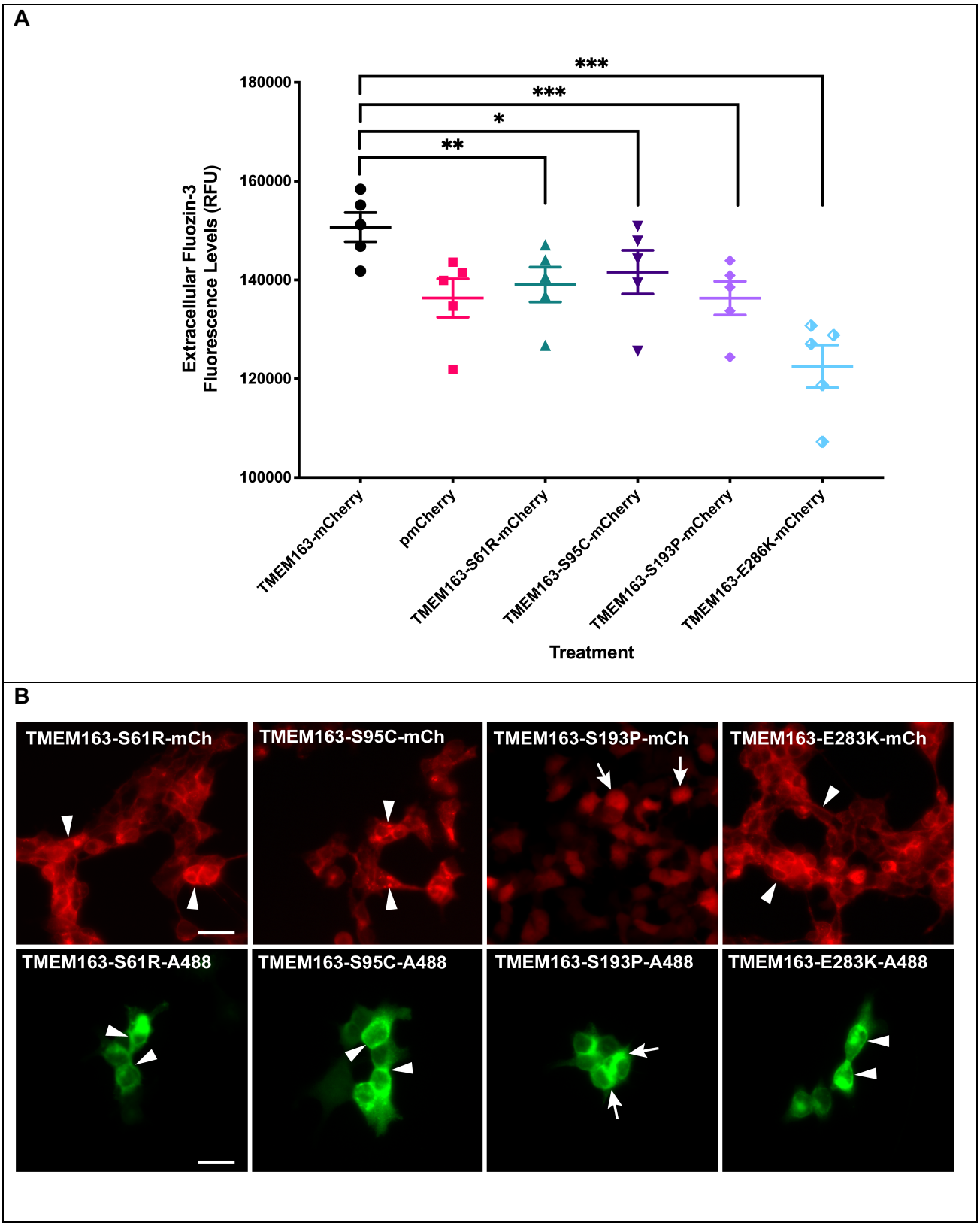
A
***
***
*
**
180000
160000
140000
120000
100000
Extracellular Fluozin-3
Fluorescence Levels (RFU)
TMEM163-mCherry
pmCherry
TMEM163-S61R-mCherry
TMEM163-S95C-mCherry
TMEM163-S193P-mCherry
TMEM163-E286K-mCherry
Treatment
B
TMEM163-S61R-mCh
TMEM163-S95C-mCh
TMEM163-S193P-mCh
TMEM163-E283K-mCh
TMEM163-S61R-A488
TMEM163-S95C-A488
TMEM163-S193P-A488
TMEM163-E283K-A488

Fig. 4

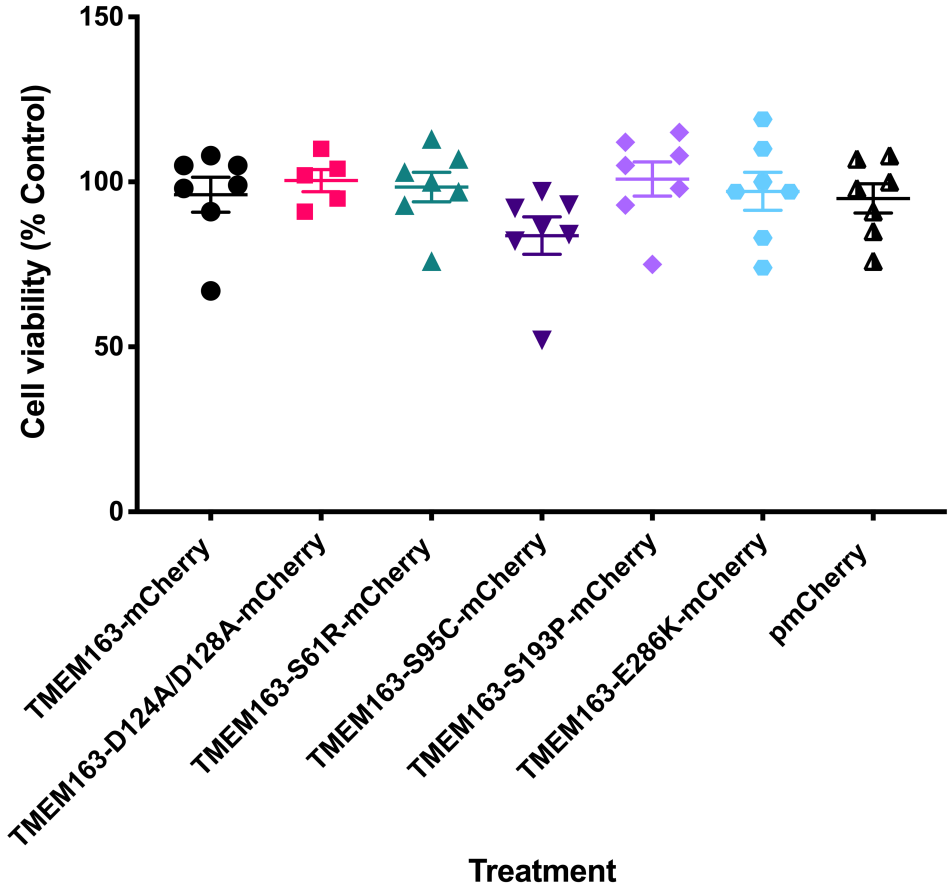
150
100
50
0
Cell viability (% Control)
TMEM163-mCherry
TMEM163-D124A/D128A-mCherry
TMEM163-S61R-mCherry
TMEM163-S95C-mCherry
TMEM163-S193P-mCherry
TMEM163-E286K-mCherry
pmCherry
Treatment

Fig. 5

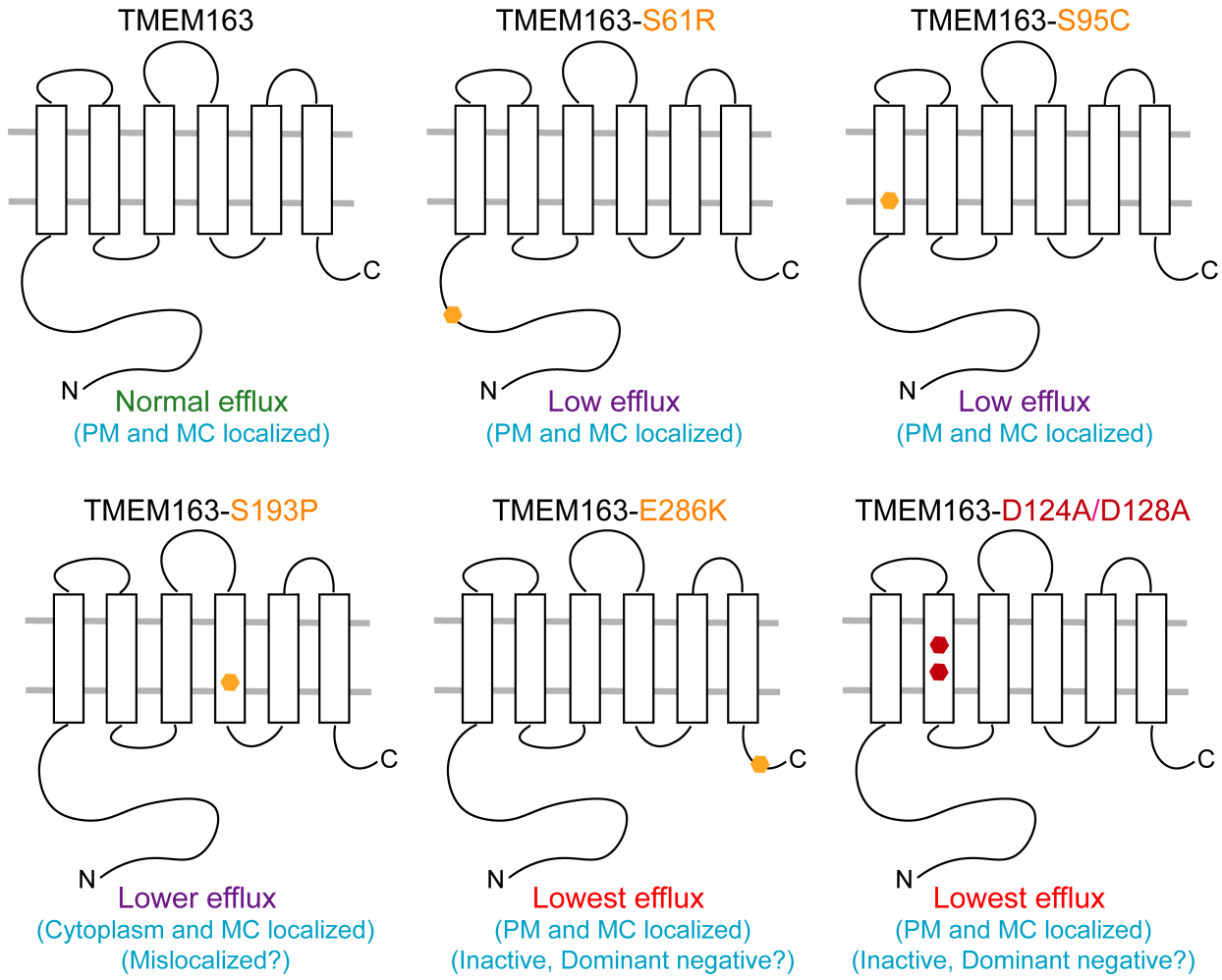
TMEM163
N
C
Normal efflux
(PM and MC localized)
TMEM163-S61R
N
C
Low efflux
(PM and MC localized)
TMEM163-S95C
N
C
Low efflux
(PM and MC localized)
TMEM163-S193P
N
C
Lower efflux
(Cytoplasm and MC localized)
(Mislocalized?)
TMEM163-E286K
N
C
Lowest efflux
(PM and MC localized)
(Inactive, Dominant negative?)
TMEM163-D124A/D128A
N
C
Lowest efflux
(PM and MC localized)
(Inactive, Dominant negative?)